AD-A113 168 NAVAL SURFACE WEAPONS CENTER DAHLGREN VA F/G 17/9
EXPERIMENTAL TIME-DOMAIN DETERMINATION OF COMPLEX RESONANCES OF--ETC(U)
DEC 81 B Z HOLLMANN, E D BALL
UNCLASSIFIED NSWC/TR-80-414 NL

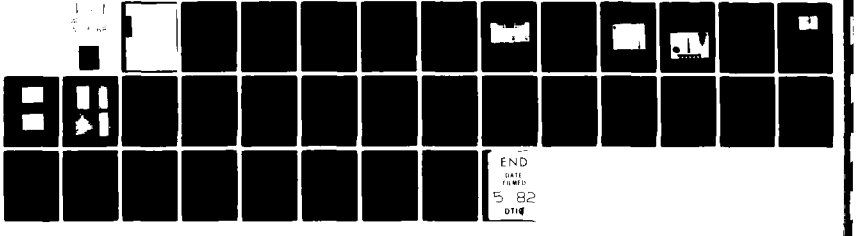

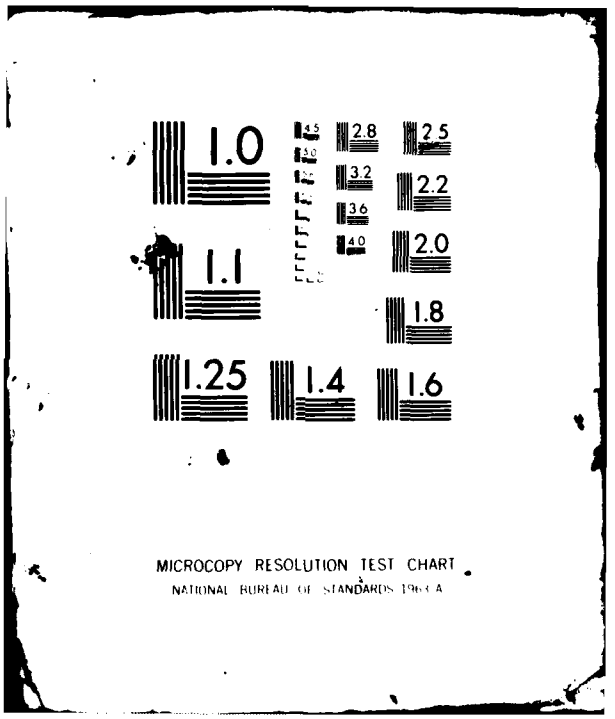
1.0
1.1
1.25
1.4
1.6
1.8
2.0
2.2
2.5
2.8
3.2
3.6
4.0
4.5
5.0
MICROCOPY RESOLUTION TEST CHART
NATIONAL BUREAU OF STANDARDS 1963 A

UNCLASSIFIED

SECURITY CLASSIFICATION OF THIS PAGE (When Data Entered)

REPORT DOCUMENTATION PAGE		READ INSTRUCTIONS BEFORE COMPLETING FORM
1. REPORT NUMBER NSWC TR 80-414	2. GOVT ACCESSION NO.	3. RECIPIENT'S CATALOG NUMBER
4. TITLE (and Subtitle) EXPERIMENTAL TIME-DOMAIN DETERMINATION OF COMPLEX RESONANCES OF SIMPLE OBJECTS		5. TYPE OF REPORT & PERIOD COVERED Final 6. PERFORMING ORG. REPORT NUMBER
7. AUTHOR(s) Bruce Z. Hollmann Edwin D. Ball		8. CONTRACT OR GRANT NUMBER(s)
9. PERFORMING ORGANIZATION NAME AND ADDRESS Naval Surface Weapons Center (F12) Dahlgren, VA 22448		10. PROGRAM ELEMENT, PROJECT, TASK AREA & WORK UNIT NUMBERS 61153N; WR02101; WR02101
11. CONTROLLING OFFICE NAME AND ADDRESS Naval Surface Weapons Center Dahlgren, VA 22448		12. REPORT DATE December 1981 13. NUMBER OF PAGES 36
14. MONITORING AGENCY NAME & ADDRESS(if different from Controlling Office)		15. SECURITY CLASS. (of this report) UNCLASSIFIED 15a. DECLASSIFICATION/DOWNGRADING SCHEDULE

16. DISTRIBUTION STATEMENT (of this Report)

Approved for public release; distribution unlimited.

17. DISTRIBUTION STATEMENT (of the abstract entered in Block 20, if different from Report)

18. SUPPLEMENTARY NOTES

19. KEY WORDS (Continue on reverse side if necessary and identify by block number)

time-domain range
Prony's algorithm
subnanosecond pulse

20. ABSTRACT (Continue on reverse side if necessary and identify by block number)

The time-domain range for transmitting a subnanosecond pulse and recording its return from a conducting object is described in this report. The advantages and problems associated with Prony's algorithm are given; the effort and progress toward overcoming the problems are described; and the results of applying Prony's algorithm to the returns from a hemisphere and a cylinder are shown. The areas of need, both theoretical and experimental, are detailed herein.

DD FORM 1 JAN 73 1473 EDITION OF 1 NOV 65 IS OBSOLETE
S/N 0102-LF-014-6601

UNCLASSIFIED

SECURITY CLASSIFICATION OF THIS PAGE (When Data Entered)

FOREWORD

The work described in this report was sponsored by the Independent Research (IR) Board of the Naval Surface Weapons Center (NSWC). It was performed during the period October 1976 to September 1979.

The traditional uses of radar have been to locate a target and to track its direction and velocity. In recent years, interest in a third use of radar has evolved: to identify an object from the scattered return. The ultimate purpose of this work, which is presently continuing, is to devise a method for identifying a complex object from the return of a radiated impulse or other suitably shaped short pulse. In order to be able to do this, the impulse response radiation of simple objects must be studied to ascertain the relationships between the shape of an object, the material of which it is made, its aspect angle, etc., and the scattered return.

This report describes the NSWC time-domain range returns from simple objects and first attempts to process them. Prony's algorithm is described and efforts to improve it are detailed. The application of Prony's algorithm to the returns is described and the results are shown. Problems with clutter and noise are discussed, and directions for future efforts are recommended.

The ultimate outcome could result in a radar target identification system, which would be of use to all the military services.

The authors wish to gratefully acknowledge the helpful critiques and encouragement of Dr. Ronald J. Gripshover, in particular, and of the NSWC IR Board, in general.

This report has been reviewed by W. S. Orsulak, Head, Special Applications Branch, and K. C. Baile, Head, Advanced Projects Division.

Released by:

DAVID B. COLBY, Head
Electronics Systems Department

TABLE OF CONTENTS

LIST OF ILLUSTRATIONS

LIST OF TABLES

INTRODUCTION

The objective of this project is to devise a method for the identification of complex objects, based on the time-domain returns from a radiated short (subnanosecond) pulse. This report details the present status of the project; describes the time-domain range and experimental apparatus; describes the present status of the apparatus and the needs for refinement and improvement. The signal processing is discussed, and in particular, the problems with Prony's algorithm are stated and the improvements to the algorithm for coping with the problems are given. The results of applying these to synthetic waveforms are given and the areas of need for further effort pointed out. An attempt to apply the algorithm to experimental data is described, and the results thereof are discussed. Finally, directions for further effort are suggested.

BACKGROUND

Baum[1] expanded the solution of a free-radiating shape (no forcing function) in terms of its singularities, or complex resonances, in the Laplace (complex frequency or "s") domain. His expansion, for finite-size objects, takes the form

$$F(s) = \sum_{i=1}^{N} \frac{A_i}{s - s_i} \tag{1}$$

where the s_i are the complex resonances or poles of the waveform, and the A_i are the coefficients or residues. In theory, the number of resonances, N, is infinity, but, in practice, the high-frequency resonances have negligibly small residues that render them undetectable. Hence, a finite number of resonances are considered. Baum showed that the poles, s_i, depend upon the object: its size, its shape, and the material of which it is made. He also showed that the residues, A_i, depend upon the initial waveform: its shape, polarization, and coupling to the object. The A_i also depend upon the aspect angle of the object in relation to the transmitter. Note that the poles, s_i, depend only upon the object and are independent of the transmitted waveform. This theoretically means that we can observe the same set of resonances, independent of the direction the observer is from the object.

If we take the inverse Laplace transform of Equation (1), we have

$$f(t) = \sum_{i=1}^{N} A_i e^{s_i t} \tag{2}$$

This is just the sum of a set of complex exponential terms. The poles, s_i, have negative real parts. That is, the free-radiating waveform must damp out in the absence of new energy supplied to the object. The function, f(t), is real, since it is a physical observable.

Prony's algorithm[2] is a method for extracting the poles and residues from a waveform of the form of Equation (2). The aim is to apply this algorithm to the time-domain radiation from an object to extract its poles.

EXPERIMENTATION

The data gathering operation is performed on a 9.1-m (30-ft) diameter ground plane shown in Figure 1. The ground plane is constructed of aluminum plates welded together to form a continuous conducting surface.

Figure 1. Time-Domain Range

The electronic apparatus, located beneath the ground plane, is shown in Figure 2. The generator is an IKOR R-100 impulse generator, which puts out a subnanosecond Gaussian pulse with an amplitude of approximately 1 kV. The repetition rate is approximately 100 Hz. At the output of the impulse generator is an FXR feedthrough capacitive pickoff probe, the output of which delivers a trigger pulse, through appropriate attenuation, to a sampling oscilloscope. The signal must go through a delay line in order to allow the sampling scope time to initiate the trace on receipt of the trigger pulse. This delay line consists of about 15.2 m (50 ft) of RG-331 cable. After the delay cable, there is a measuring probe, which was designed and built by IKOR. It is a capacitive feedthrough probe with an attenuation of 49 ±1 dB and a flat frequency response from 5 MHz to 3 GHz. After this probe, an RG-9 cable, approximately 0.8-m (2.5-ft) long carries the signal to the base of the transmitter

antenna. With the exception of the output of the impulse generator and the FXR pickoff probe, which uses Type N connectors, the connectors from the generator to the base of the transmitter antenna are all of type HN. This type of connector was chosen in anticipation of future higher voltages.

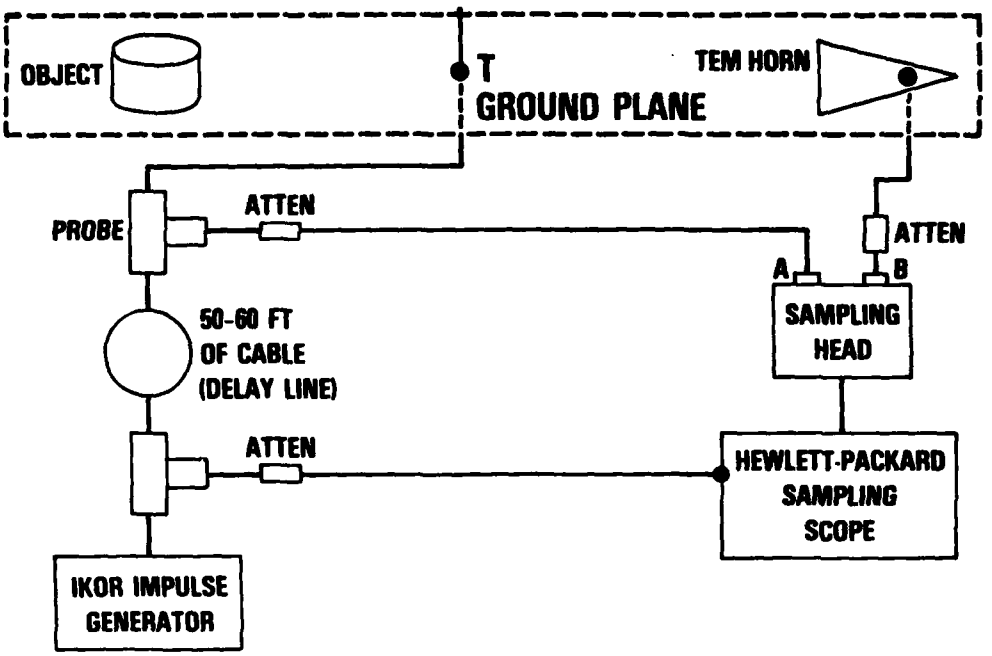

Figure 2. Experimental Apparatus

The transmitter antenna is a 5.2-m (17-ft) wire monopole. Its upper end is supported from the ceiling. The pulse is radiated by the monopole and received by the receiving antenna. Meanwhile, the radiated pulse strikes the object, giving a return from the object that arrives at the receiving antenna a few nanoseconds after the initial pulse.

The receiving antenna is a half TEM horn, 0.3-m (1-ft) long connected to the stub of a Type N wall connector mounted in the ground plane. The other half of the TEM horn is imaged by the ground plane. This simulates a TEM horn with an angle of 16°. These particular antennas (monopole transmitter and TEM horn receiver) were chosen as a start because the monopole transmits with high fidelity the source waveform, while the TEM horn receives and reproduces with high fidelity the waveform of the electric field of the radiation. Reference 3 gives the details of various antenna configurations as transmitters and receivers.

Figure 3 shows the relative positioning of the transmitter (monopole), the receiver (TEM horn), and the object. (The paint can shows the position of the object.) They were positioned in line so as to simulate a monostatic system; i.e., the object is in the same direction from both transmitter and receiver. A check revealed that the presence of the transmitter between the receiver and object does not affect returns within the sensitivity of the instrumentation. The distance between the monopole and the TEM horn is 2.3 m (7.5 ft). The reason for this distance is to protect the receiving equipment from the amplitude of the transmitted pulse, until appropriate duplexing equipment can be built. The part of the object nearest the transmitter is 0.6 m (2 ft) from the transmitter. This will assure a delay of about 4 nsec from the time the radiated pulse is received by the TEM horn until the return from the object arrives. (Light travels 30 cm in 1 nsec). This 4-nsec delay is necessary to allow for the trail-off from the transmitted pulse.

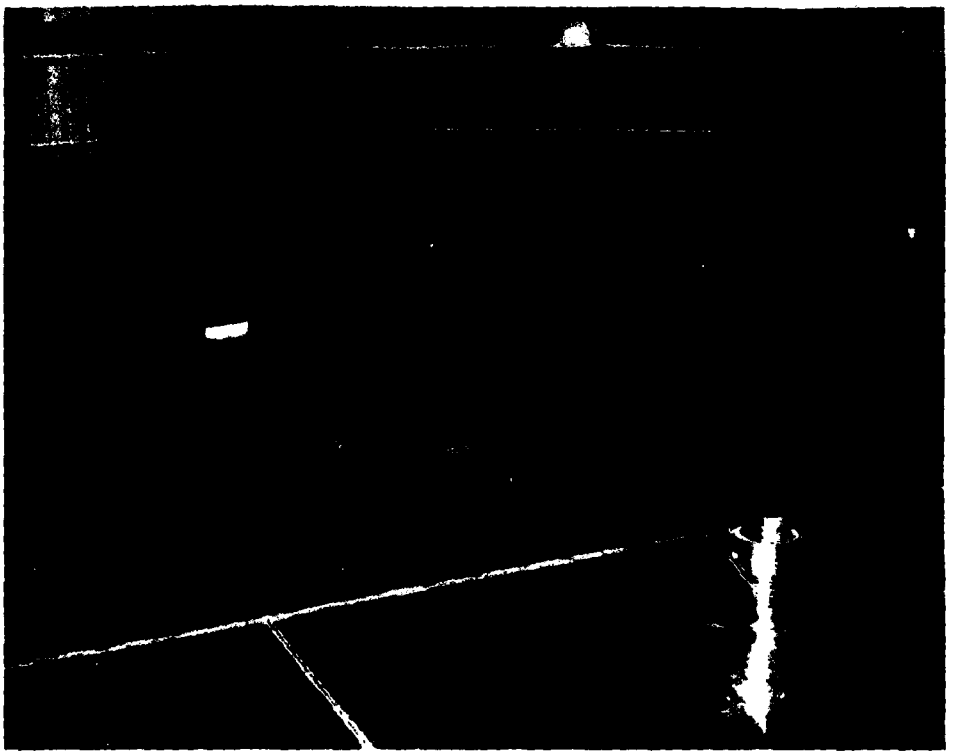

Figure 3. Relative Positioning of Transmitter (center), Receiver (upper left), and Object (lower right)

Upon receipt by the TEM horn, the signal is fed to a sampling oscilloscope through an RG-9 cable and appropriate attenuators. The sampling oscilloscope is a Hewlett-Packard Model 181A dual-beam oscilloscope. It has a Model 1811A sampling time base and vertical amplifier plug-in. The sampling head is a Model 1430C. All connectors in the receive circuit are of Type N.

On the back of the sampling scope's main frame are outputs for monitoring waveforms by external recording equipment. The waveforms that can be monitored are the two traces displayed on the screen and the horizontal sweep (sawtooth) waveform. A Hewlett-Packard 3960 analogue tape recorder was used to record the waveforms for later data reduction on a PDP 1145 computer. The idea was to record about 30 traces of the returns from each object and later to have the computer digitize the returns and compute an average for each return. A major advantage of using an analogue tape recorder is that the original traces would be recorded permanently and could be referred to as often as needed. However, the tape recorder, even within the manufacturer's specification and with the use of filters, puts out noise at such a level as to render proper digitizing and averaging of data extremely difficult and uncertain. Therefore, to obtain results for this report, traces of returns were enlarged to 30.5 cm (12 in.) by 38.1 cm (15 in.) and hand digitized. More will be said about this process later.

The objects whose returns are being studied are a hemisphere, a cone, and a cylinder, which are shown in Figure 4. They are each 12.7 cm (5 in.) in diameter at the base. The cone has a 30° angle, and the cylinder is 25.4 cm (10 in.) in height. They are all solid aluminum.

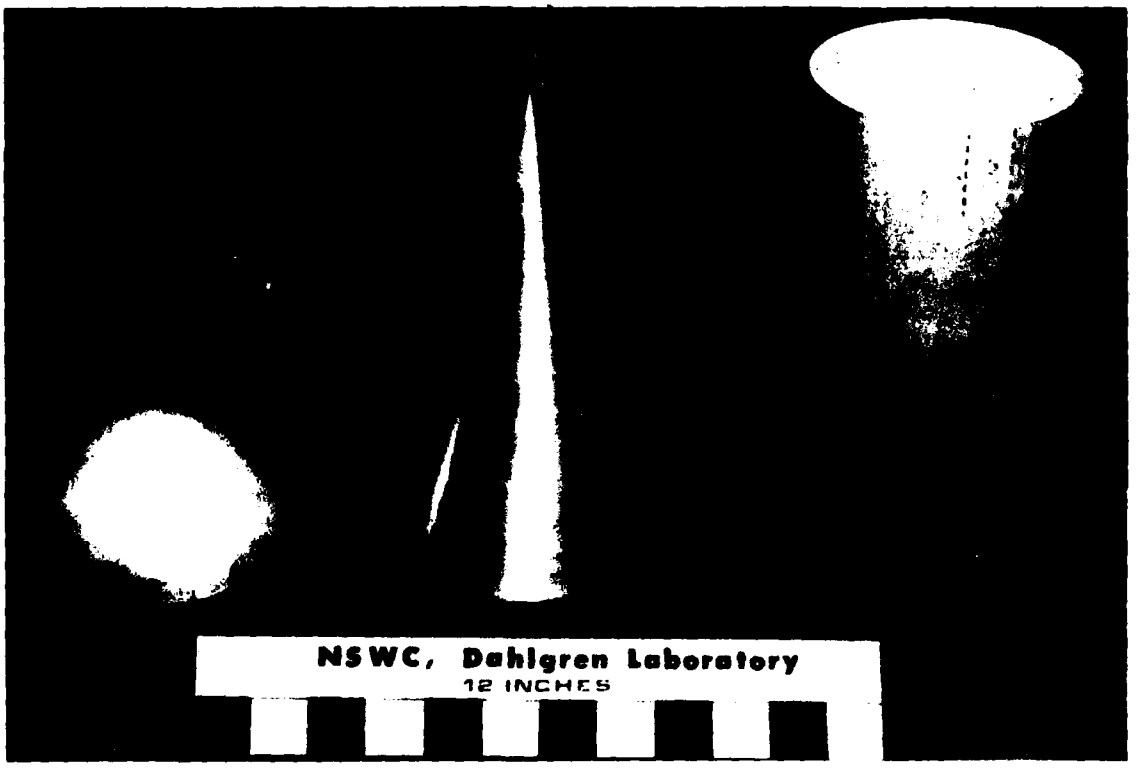

Figure 4. Hemisphere, Cone, and Cylinder

Figure 5 shows sampling oscilloscope traces of the impulse generator pulse. Figure 5a shows it as monitored by the IKOR probe at the output of the delay line and just before transmission by the monopole antenna. Figure 5b shows the pulse as received by the TEM horn receiving antenna. The wiggles in the trailoffs of these traces arise from reflections caused by connectors in the transmission lines to and from the antennas.

Figure 6 shows sampling oscilloscope traces of waveforms in the transmitter (IKOR probe) and receiver (TEM horn) circuits, with no object on the ground plane. The lower trace shows the waveforms in the transmitter circuit. The first pulse in the lower trace is the initial impulse generator pulse as seen in Figure 5a. The second pulse is the reflection of the initial pulse at the base of the transmitter monopole. Notice the third pulse that appears about 40 nsec after the initial pulse. It represents a reflection of energy from the tip of the transmitter monopole, a distance of 5.2 m (17 ft) from the base. The upper trace shows the waveforms in the receiver circuit. The first pulse is the impulse generator pulse. After its trailoff, except for clutter, there is a clear time window of about 20 nsec. The first small negative peak, just after the second vertical grid line to the right from the center, is a reflection from the nearest wall of the building. The large oscillations immediately after that are caused by ringing by the transmitter monopole antenna and reflections from the ground plane edges and building walls. Figure 7 shows the same waveforms as Figure 6 except that the aluminum cylinder is placed in the object position. No changes are seen in the lower trace (the transmitter circuit waveform). The upper trace (the receiver circuit waveform) is the same as before, except that the return from the cylinder is seen, immediately after the impulse generator pulse trailoff. The pictures of traces from target returns will show the 10-nsec-time window from the third (from the left) to the fifth (center) grid line of Figure 7.

Figure 8 shows expanded traces of returns from the cylinder, the cone, and the hemisphere. The trace marked "clutter" is what is seen in the same timeframe when no object is present. These photographs were enlarged to 30.5 cm (12 in.) by 38.1 cm (15 in.) in such a way as to make the squares of the grids the exact same size. Xerox copies of the enlargements were made on thin paper. These copies were carefully checked for distortion by measuring the squares on the grid and comparing with the squares on the photographed enlargements. The worst distortion was found to occur near the edges, away from the important parts of the traces, which showed negligible distortion. The curves were then hand digitized from the thin-paper copies on an Elographics digitizing table. Every effort was made for even spacing along the time axis. Approximately 201 points were digitized from each curve. A cubic spline routine similar to that described in Reference 6 was used to smooth each data set and interpolate to 512 points, equally spaced along the time axis. The smoothed data sets were submitted to our CDC 6700 computer for processing.

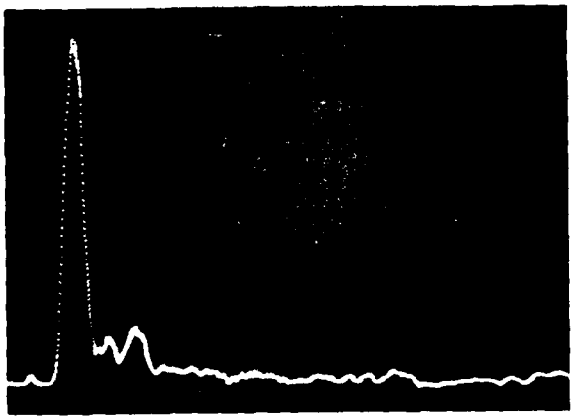

a) **BEFORE TRANSMISSION**

200 mv/div
1 ns/div

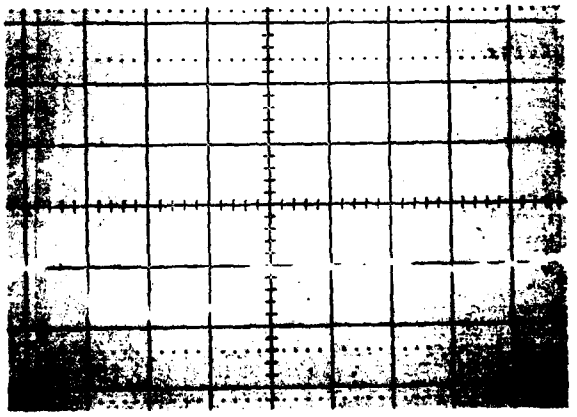

b) **RECEIVED BY TEM HORN**

Figure 5. Impulse Generator Pulse

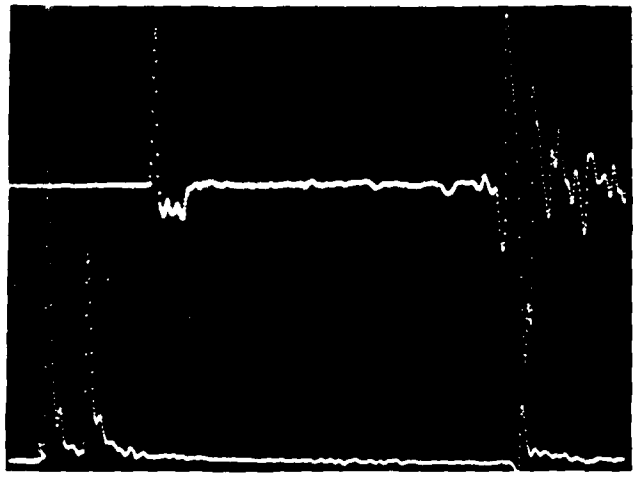

Figure 6. Transmitted and Received Waveforms; No Object on Ground Plane (5 nsec/div; 200 mV/div) (Lower trace--transmitted pulse and its reflections. Upper trace--as received by TEM Horn)

Figure 7. Transmitted and Received Waveforms; Cylinder on Ground Plane in Object Position (5 nsec/div; 200 mV/div) (Lower trace--transmitted pulse and its reflections. Upper trace--as received by the TEM horn)

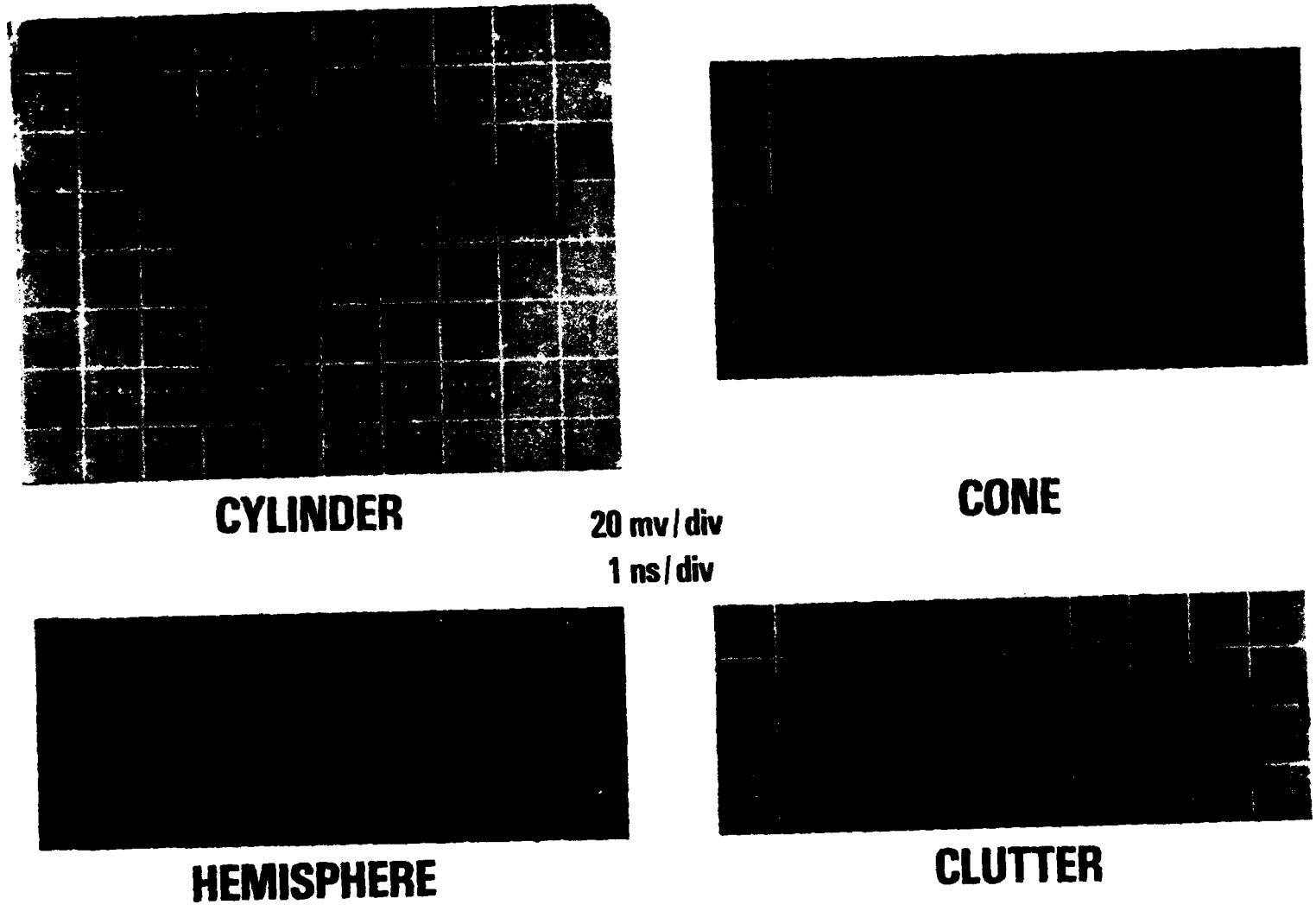

Figure 8. Returns

PRONY'S ALGORITHM

This section gives the exact method used by Prony's algorithm for determining the poles and residues of a waveform described by Equation (2). The procedure is basically that outlined in Reference 5.

Let us sample f(t) at N points, equally spaced in time. Let us set the sampling times as follows:

$$t_k = (k-1)\delta, \quad k = 1, 2, \ldots, N$$

where δ is the time interval between samples. Also, let us rewrite Equation (2) as

$$f_k \equiv f(t_k) = \sum_{m=1}^{M} A_m e^{s_m(k-1)\delta} = \sum_{m=1}^{M} A_m x_m^{k-1} \tag{3}$$

where

$$x_m = e^{s_m\delta}$$

Form the following set of equations:

$$\begin{aligned}
A_1 &+ A_2 &+ \ldots + A_M &= f_1 \\
A_1x_1 &+ A_2x_2 &+ \ldots + A_Mx_M &= f_2 \\
A_1x_1^2 &+ A_2x_2^2 &+ \ldots + A_Mx_M^2 &= f_3 \\
&&\vdots& \\
A_1x_1^{N-1} &+ A_2x_2^{N-1} &+ \ldots + A_Mx_M^{N-1} &= f_N
\end{aligned} \tag{4}$$

Let x_m represent the roots of an M^{th} order polynomial

$$\sum_{m=1}^{M+1} c_m x^{m-1} = (x-x_1)(x-x_2)\ldots(x-x_M) = \prod_{m=1}^{M}(x-x_m) \tag{5}$$

where

$$c_{M+1} = 1$$

Let us multiply the first equation of (4) by c_1, the second equation of (4) by c_2, etc., for the first M+1 equations. Then, using Equation (5), we form the equation

$$f_1 c_1 + f_2 c_2 + \ldots + f_{M+1} = 0$$

Repeat this operation, beginning with the second equation of (4), thereby forming

$$f_2 c_1 + f_3 c_2 + \ldots + f_{M+2} = 0.$$

Repeat this operation until M such equations are formed

$$\begin{aligned} f_1 c_1 + f_2 c_2 + \ldots + f_M c_M &= -f_{M+1} \\ f_2 c_1 + f_3 c_2 + \ldots + f_{M+1}\, c_M &= -f_{M+2} \\ &\vdots \\ f_M c_1 + f_{M+1} c_2 + \ldots + f_{2M-1}\, c_M &= -f_{2M} \end{aligned} \tag{6}$$

We may express Equation (6) in matrix form as follows

$$F\,\underline{C} = \underline{B}, \tag{7}$$

where

$$F = \begin{bmatrix} f_1 & f_2 & \ldots & f_M \\ f_2 & f_3 & \ldots & f_{M+1} \\ \cdot & & & \\ \cdot & & & \\ \cdot & & & \\ f_M & f_{M+1} & \ldots & f_{2M-1} \end{bmatrix}$$

the data sample matrix,

$$\underline{C} = \begin{bmatrix} c_1 \\ c_2 \\ \cdot \\ \cdot \\ \cdot \\ c_M \end{bmatrix}$$

the vector of the coefficients, and

$$\underline{B} = \begin{bmatrix} -f_{M+1} \\ -f_{M+2} \\ \cdot \\ \cdot \\ \cdot \\ -f_{2M} \end{bmatrix}$$

Equation (6) is solved for the c's. Then, we use the c's in Equation (5) to solve for the x's, from which we can obtain s_m using

$$s_m = \frac{1}{\delta} \ln x_m \tag{8}$$

The A's can be found via Equation (4).

The foregoing discussion detailed the exact procedure for calculating the poles and residues using Prony's Algorithm. If M is the number of poles to be determined, we need 2M sample data points for the exact calculation. Often, there are more than 2M data points available. When more than 2M points are used, the problem is overdetermined. The next section will describe new procedures for handling the overdetermined case.

In activating the algorithm as described, one must know in advance the number of poles or guess, if the number is not known. If the estimated number is too low, the results will be nonsense. If the estimate is too high, the algorithm will give the correct poles, plus some extra (curve-fitting) poles with low residues. However, to obtain meaningful results, the estimate must not be too far above the correct number. ANALYSIS TECHNIQUES will describe what has been done to handle these shortcomings.

ANALYSIS TECHNIQUES

The most critical procedure in Prony's method (in the overdetermined case) is finding the least-squares solution of

$$F \underline{C} = \underline{B} \tag{9}$$

for $\underline{C}$, the vector of coefficients for the polynomial. The linear least-squares procedure for solving Equation (9) for $\underline{C}$ is given in Reference 6. Once the coefficients are accurately known, finding the roots of the polynomial is generally straightforward. The residues are less important for most purposes, because they are not necessarily characteristic of the object being irradiated.

CROUT ROUTINE

The original SEMPEX program used the CROUT[7] method for finding the polynomial coefficients. In the CROUT subroutine, Equation (9) is multiplied by F^T to obtain

$$F^T F \underline{C} = F^T \underline{B} \tag{10}$$

Here, F^T is the transpose of F. The vector,

$$\underline{C}^* = (F^TF)^{-1}F^T\underline{B} \tag{11}$$

which is the unique solution of Equation (10) is the least-squares solution of Equation (9). The CROUT method uses a modification of the Gauss Reduction[7] to find the solution. It does not work well when the columns of F are close to linear dependence because the determinant of F^TF will be small and the problem nearly singular.

HFTI ROUTINE

We found the HFTI[8] routine, available in the Naval Surface Weapons Center (NSWC) Library of Mathematics Routines, to be more suitable for our purposes. It is more accurate because most inner products are computed in double precision. It is able to deal with the problem of rank deficiency when the columns of F are close to being linearly dependent. The HFTI routine can also be used to get an indication of the number of poles present in the signal. In the process of computing the least-squares solution, the HFTI routine transforms the matrix, F, to upper triangular form with an orthogonal matrix, Q, and an orthogonal permutation matrix, P, so that QFP = R, and R has zeroes below the diagonal. The matrix, P, reorders the columns so that the absolute values of the diagonal elements are monotonically decreasing. The HFTI routine then calculates a condition number $C_\#$ for this triangularized data matrix by dividing the maximum (upper left) diagonal element, a_{11}, by the minimum (lower right) diagonal element, a_{MM}. That is, $C_\# = a_{11}/a_{MM}$. The rank k of F is the number of linearly independent columns of F. If the number of columns M is greater than k, the last M-k diagonal elements of R will be 0. That is, as i is increased, a_{ii} decreases monotomically and goes abruptly to zero when i>k. In this case, $C_\# = a_{11}/a_{MM} = \infty$ for M>k. In the presence of noise, there is still an abrupt decrease in a_{ii} (and an abrupt increase in $C_\#$) as i becomes greater than k, although a_{ii} is no longer equal to zero (and $C_\# < \infty$) for i>k. As the noise is increased, the decrease in a_{ii} (and increase in $C_\#$) as i becomes greater than k, is less abrupt.

Assuming no noise in the data, the number of linearly independent columns (or the rank k) of F is usually equal to the number of poles. This is true for the following reason. Assume m is the actual number of poles, and M is the assumed number of poles with M>m. Let N be the number of data points. Now F is defined to be

$$\begin{bmatrix} f_1 & f_2 & \cdots & f_M \\ f_2 & & & \vdots \\ \vdots & & & \vdots \\ \vdots & & & \vdots \\ f_{N-M} & f_{N-M+1} & & f_{N-1} \end{bmatrix}$$

If there is no noise, then

$$f_j = \sum_{k=1}^{m} A_k x_k^j \tag{12}$$

where

$$\sum_{n=1}^{m} C_n x_k^{n-1} + x_k^m = 0 \tag{13}$$

Denote the j 'th column of F by $\underline{F}_j$. By Equation (12)

$$\underline{F}_j = \begin{bmatrix} \sum_{k=1}^{m} A_k x_k^j \\ \sum_{k=1}^{m} A_k x_k^{j+1} \\ \vdots \\ \sum_{k=1}^{m} A_k x_k^{j+N-M-1} \end{bmatrix}$$

By Equation (13)

$$\sum_{n=1}^{m} C_n \underline{F}_{n-n} + \underline{F}_{-m+1} = \underline{0}. \tag{14}$$

Thus, the number of linearly independent columns cannot be greater than m. It is possible that there could be fewer than m, but this would be very unusual.

Thus, if the number of linearly independent columns of F is m, the rank of F is m and the last M-m diagonal elements of R would be 0 in the absence of noise. We could then conclude that the number of poles is probably m and restart the algorithm assuming m poles instead of M.

In practical work, we check to see when M becomes greater than m by monitoring the condition number $C_\#$ of matrix R. In successive runs, we note the value of M when $C_\#$ undergoes an abrupt increase. The rank m is then M-1, the value of M just before $C_\#$ increases suddenly. When $C_\#$ is large (usually greater than 100 in practical situations), we say that the data matrix is ill-conditioned.

If the signal is contaminated by noise, as is usually the case, the situation is somewhat different. If the noise is random, uncorrelated noise, the columns of F will be linearly independent because the noise samples are independent of one another. Thus, the rank of F will be M and none of the diagonal elements of R will be 0. However, if the noise level is relatively small, the last M-m diagonal elements will be much smaller than the other diagonal elements. How large then must one set the tolerance for the diagonal elements to

determine how many poles are actually present? Note that the matrix, Q, because of its orthogonality, does not alter the norm of the columns of F. The matrix, P, merely reorders the columns where necessary, so it can be ignored for this dicussion.

Assume the diagonal element in column j would be 0, if no noise were present. Note that Q will be somewhat different when noise is present. Because of the noise, the k'th element of $\underline{F}_j$ will be $f_{j+k-1} + N_{j+k-1}$ where N_{j+k-1} is the noise. If the noise is random with mean 0 and variance σ_N^2, then

$$E\left\{\sum_{k=1}^{N-M}(f_{j+k-1} + N_{j+k-1})^2\right\} = \sum_{k=1}^{N-M} f_{j+k-1}^2 + (N-M)\sigma_N^2 \tag{15}$$

where E denotes expected value. The effect of Q will be to redistribute this quantity in the column $Q\underline{F}_j$ so that all elements below the j'th or diagonal element will be 0. Let us write the k'th element of $Q\underline{F}_j$ as $r_{kj} + e_{kj}$ where r_{kj} is the value the element would have, if there were *no* noise. Because of conservation of the norm by Q,

$$\sum_{k=1}^{j} r_{kj}^2 = \sum_{k=1}^{N-M} f_{j+k-1}^2 \tag{16}$$

with $r_{jj} = 0$, and

$$E\left\{\sum_{k=1}^{j}(r_{kj} + e_{kj})^2\right\} = \sum_{k=1}^{N-M} f_{j+k-1}^2 + (N-M)\sigma_N^2 \tag{17}$$

These two equations somewhat justify the approximation

$$j \cdot E\left\{e_{jj}^2\right\} \approx (N-M)\sigma_N^2 \tag{18}$$

or

$$\sqrt{E(e_{jj}^2)} = \sigma(e_{jj}) \approx \sqrt{\frac{N-M}{j}}\,\sigma_N \tag{19}$$

Assuming j = M, then

$$\sigma(e_{jj}) \approx \sqrt{\frac{N-M}{M}}\,\sigma_N \tag{20}$$

If the diagonal element of the last column of QFP is smaller than this, the number of poles is probably less than M.

NONLINEAR LEAST SQUARES

Contrary to what one might assume, the normal linear least-squares method does not give the best fit to the data. Written in terms of the estimated solution for the polynomial coefficients $\hat{\underline{C}}$ and the error of the fit $\underline{d}$, Prony's equation is

$$F\,\hat{\underline{C}} = \underline{B} + \underline{d} \tag{21}$$

The usual linear least-squares solution minimizes the norm of $\underline{d}$. This is the error in $\underline{B}$, which does not involve all of the data values. Also, there are actually $2M$ parameters of the problem: the M poles and the M residues. The linear least-squares method optimizes only M parameters simultaneously.

The nonlinear least-squares method of Evans and Fischl[4] avoids these drawbacks at the expense of a great deal of extra computation. It is based on Equation (21) and on

$$\underline{f} = F_1\,\underline{A} + \underline{e}$$

$$\text{with } \underline{f} = \begin{bmatrix} f_1 \\ \cdot \\ \cdot \\ f_n \end{bmatrix}$$

$$\text{and } F_1 = \begin{bmatrix} 1 & 1 & \cdots & 1 \\ x_1 & x_2 & & x_M \\ \cdot & \cdot & & \cdot \\ \cdot & \cdot & & \cdot \\ \cdot & \cdot & & \cdot \\ x_1^{N-1} & x_2^{N-1} & & x_M^{N-1} \end{bmatrix} \tag{22}$$

Here, $\underline{e}$ is the error vector involving the error in fitting all the data to be minimized by a simultaneous optimization of $\underline{C}$ and $\underline{A}$. Equation (21) can be rewritten

$$B^T\,(\hat{\underline{C}})\,\underline{f} = \underline{d} \tag{23}$$

by defining the N x (N-M) matrix

$$B(\underline{C}) = \begin{bmatrix} C_1 & 0 & 0 & \cdots & 0 \\ C_2 & C_1 & 0 & & 0 \\ \cdot & \cdot & C_1 & & \cdot \\ \cdot & \cdot & \cdot & & \cdot \\ \cdot & \cdot & \cdot & & \cdot \\ C_M & \cdot & \cdot & & C_1 \\ 1 & C_M & \cdot & & C_2 \\ 0 & 1 & C_M & & \cdot \\ \cdot & 0 & 1 & & \cdot \\ \cdot & \cdot & 0 & & C_M \\ 0 & \cdot & & & 1 \end{bmatrix}$$

There is a corresponding equation for noise-free data $\underline{h}$ and the correct values of $\underline{C}$ and no error.

$$B^T(\underline{C})\ \underline{h} = \underline{0} \tag{24}$$

It follows then that

$$B^T\ \underline{e} = B^T\ (\underline{f}-\underline{h}) = \underline{d} \tag{25}$$

The problem is given $\underline{d}$ to find $\underline{e}$. There is no unique solution to this as it is an underdetermined problem because B^T has more columns than rows. This represents a set of N-M equations in N unknowns. Another way to look at this is that $\underline{d}$ is a function of the M elements of $\underline{C}$, while $\underline{e}$ is a function of $\underline{C}$ and additionally of the M elements of $\underline{A}$. The solution can be made unique by constraining $\underline{A}$ to be a function of $\underline{C}$. The optimal way to do this is, for a given $\underline{C}$, define $\underline{A}^*(\underline{C})$ to be that which minimizes the norm of $\underline{e}(\underline{C}, \underline{A}^*)$. Then there will be a matrix $W(\underline{C})$ such that

$$\underline{e}(\underline{C}, \underline{A}^*) = W(\underline{C})\ \underline{d}(\underline{C}) \tag{26}$$

Evans and Fischl show that $W(\underline{C})$ is given by

$$W(\underline{C}) = B(\underline{C}) \left[B^T(\underline{C})\ B(\underline{C})\right]^{-1} \tag{27}$$

The strategy for the nonlinear least-squares method is to solve iteratively for the value of $\underline{C}$ that will minimize $\underline{e}(\underline{C},\underline{A}^*)$ in Equation (26). The algorithm begins by solving the linear least-squares problem of Equation (21). The solution of this is

$$\underline{C}^{(0)} = (F^T F)^{-1} F^T \underline{B} \tag{28}$$

Then, we find

$$W^{(0)}(\underline{C}^{(0)}) = B(\underline{C}^{(0)}) \left[B^T(\underline{C}^0) B(\underline{C}^0) \right]^{-1} \tag{29}$$

Define $\underline{C}^{(1)}$ as the vector that minimizes the norm of $\underline{e}$ in the equation

$$\underline{e}(\underline{C}) = W^{(0)} \underline{d}(\underline{C}) = W^{(0)} (F\,\underline{C} - \underline{B}) \tag{30}$$

The solution will be

$$\underline{C}^{(1)} = \left[F^T W(0)^T W(0) F \right]^{-1} F^T W(0)^T W^{(0)} \underline{B} \tag{31}$$

This solution for $\underline{C}^{(1)}$ can then be used to compute $W^{(1)}(\underline{C}^{(1)})$, which can be used in the least-squares equation

$$\underline{e}(\underline{C}) = W^{(1)}(F\,\underline{C} - \underline{B}) \tag{32}$$

to find an improved estimate $C^{(2)}$. This procedure can be reiterated as many times as accuracy requires and funds allow. Evans and Fischl follow this procedure with a gradient method to further refine the solution. This was introduced primarily for mathematical completeness and is generally not necessary in practical applications. It was not included in our application of the algorithm.

KALMAN FILTER

An alternative to the nonlinear least-squares technique is a sequential estimation method based on Kalman Filter Theory.[9] It has apparently never been applied to this problem before but shows considerable promise for situations where multiple independent returns are available. In these situations, it can exceed the accuracy of the nonlinear least-squares method with computer memory requirement comparable to linear least squares. It achieves this by sequentially processing the data in small blocks, in the end obtaining the equivalent of one simultaneous solution for all the data sets. The data sets can involve signals with different residues and different data spacing as long as the poles are the same.

The way this method works is as follows. Assume we have K subsets of data, each of which satisfies Prony's equation

$$\begin{array}{llll} ((N_j-M)\times M) & (M) & (N_j-M) & (N_j-M) \end{array} \quad \text{(dimensions of matrices and vectors below)}$$

$$F^{(j)} \quad \underline{C} = \underline{B}^{(j)} + \underline{d}^{(j)} \qquad j = 1, 2, \ldots, K \tag{33}$$

Here, $F^{(j)}$ is the j'th data matrix of dimension N_j-M by M, $\underline{C}$ is the vector of the polynomial coefficients of dimension M, $\underline{B}^{(j)}$ is the j'th $\underline{B}$ vector of dimension N_j-M and $\underline{d}^{(j)}$ is the error vector also of dimension N_j-M. Now assume that all the data contain the same set of poles, and, thus, the polynomial coefficients $\underline{C}$ should ideally be the same. The object is to obtain, using all the data sets, the solution for $\underline{C}$ that will give the smallest value of $\sum_{j=1}^{k} \left| \underline{d}^{(j)} \right|^2$; i.e., the overall unweighted (linear) least-square error.

It should be noted here that the theory allows for the minimization of a weighted sum of squared errors. To obtain the minimum variance solution, what must be minimized is $\underline{D}^T W \underline{D}$ where $\underline{D}$ is a column vector made up of all the $\underline{d}^j$'s and $W^{-1} = E(\underline{D}^T\underline{D})$, the expectation value of D^TD. In our application, however, the errors are assumed to be independent and to have equal variance. Therefore, W becomes a constant times the identity matrix and has no effect on the theory.

The k'th estimate for $\underline{C}$, denoted $\underline{C}^{(k)}$ represents the simultaneous least-squares solution of the first k subsets of data. To continue the process and find $\underline{C}^{(k+1)}$ also requires knowing $P^{(k)}$, which is the covariance matrix of the current estimate $\underline{C}^{(k)}$. According to the Kalman theory, the solution is

$$\underline{C}^{(k+1)} = \underline{C}^{(k)} + P^{(k)}F^{(k+1)^T}(I+F^{(k+1)}P^{(k)}F^{(k+1)^T})^{-1}(\underline{B}^{(k+1)} - F^{(k+1)}\underline{C}^{(k)}) \quad (34)$$

$$P^{(k+1)} = P^{(k)} - P^{(k)}F^{(k+1)^T}(I+F^{(k+1)}P^{(k)}F^{(k+1)^T})^{-1}F^{(k+1)}P^{(k)} \quad (35)$$

Note that the inverse is of dimension $(N_k-M)X(N_k-M)$.

The iteration begins by computing

$$P^{(1)} = (F^{(1)^T}F^{(1)})^{-1} \quad (36)$$

$$\underline{C}^{(1)} = P^{(1)}F_1{}^T\underline{B}^{(1)} \quad (37)$$

In theory the number of data points N_k could be different for each data subset and could be any number $\geq 2M$. In our application, we use $N_k = 2M$ points for every data set. This simplifies the computation somewhat and reduces the dimension of the inverse to M x M. In comparison, the nonlinear least-squares method involves inverses of dimension (N-M) x (N-M). Thus, for example, if M = 14 and N = 84, the dimension of the nonlinear least squares inverses would be 70 x 70, involving 4900 elements, whereas the Kalman method would do this in three steps with each step involving inverses of dimension 14 x 14, or 196 elements per step.

APPLICATIONS

APPLICATION TO SYNTHETIC DATA

All of the above methods work well, if the noise level is low and if certain criteria on data spacing are met. We have found by experience that the data spacing Δt must be small enough to satisfy the Nyquist criterion that $\frac{1}{2\Delta t}$ be greater than or equal to the highest frequency present. Another finding is that the total data span, T, must be large enough so that $\frac{1}{T}$ is less than or equal to the lowest frequency present. These criteria both seem reasonable on theoretical grounds. There have been cases where the method worked without satisfying one of these criteria but usually it does not. A large condition number is often an indication of trouble in this area.

The true test of these methods is their performance in the presence of noise. In order to compare them, we have used a set of six pairs of poles published by Van Blaricum and Mittra.[10] In this report, they present a method that works on synthetic data generated from these poles using residue values of 1.0 in the presence of additive random Gaussian noise with a standard deviation σ as large as $\sigma_N = 0.01$. With our methods, we are able to get reasonable results with $\sigma_N = 0.1$.

The criterion we used to measure the effectiveness of the above described methods in noise is the root of the sum of the squares (RSS) of the differences between our calculated and Van Blaricum's poles. That is,

$$RSS = \sqrt{\sum_i \left| s_i - \hat{s}_i \right|^2} \tag{38}$$

where $\hat{s}_i$ are Van Blaricum's poles and s_i are the poles as determined by our methods. The lower RSS is, the more effective the method.

Table 1 shows results obtained with the three methods on synthetic data generated from Van Blaricum's poles, using the residues shown in Table 2. Random uncorrelated Gaussian noise was added with a σ_N of 0.1. Each synthetic return had an independent noise sample; thus, cases 1 and 2, which had the same poles and residues gave different results. Data spacing Δt was 0.25 nsec.

The Kalman method was used to analyze the data in the following manner:

Iteration	Data Sets Used
1	1
2	1 and 2
3	1, 2, and 3
4	1, 2, 3, and 4
5	1, 2, 3, 4, and 5

Results improved with each iteration, as more data sets were included. In these calculations, the Kalman method used 150 points from each return (data set) while the other methods used only 80 points each.

Table 1. Results from Synthetic Data (Van Blaricum and Mittra)

$$\sigma_N = 0.1$$

$$RSS = \sqrt{\sum_i \left| s_i - \hat{s}_i \right|^2}$$

Case No./Method	Linear-Least Squares	Nonlinear-Least Squares	Kalman
1	0.0302	0.0261	0.0543
2	0.0382	0.0279	0.0438
3	0.0116	0.0097	0.0262
4	0.0246	0.0234	0.0155
5	0.0385	0.0391	0.0106

Table 2. Poles and Residues

Poles/Case No.	Residues 1	2	3	4	5
-0.082 ± j 0.926	-0.70 ± j 0.70	-0.70 ± j 0.70	0.70 ± j 1.0	0.70 ∓ j 0.70	-1.0 ± j 0.0
-0.147 ± j 2.874	-0.70 ± j 0.70	-0.70 ± j 0.70	0.70 ± j 1.0	-0.70 ± j 0.70	0.70 ∓ j 0.70
-0.188 ± j 4.835	-0.70 ± j 0.70	-0.70 ± j 0.70	0.70 ± j 1.0	0.70 ∓ j 0.70	0.70 ∓ j 0.70
-0.220 ± j 6.800	0.70 ± j 0.70	0.70 ± j 0.70	0.00 ± j 1.0	-0.70 ± j 0.70	1.0 ± j 0.0
-0.247 ± j 8.767	0.70 ± j 0.70	0.70 ± j 0.70	0.00 ± j 1.0	0.70 ∓ j 0.70	0.0 ∓ j 1.0
-0.270 ± j 10.733	0.70 ± j 0.70	0.70 ± j 0.70	0.00 ± j 1.0	-0.70 ± j 0.70	-0.70 ± j 0.70

It can be seen that all three methods performed rather well. The nonlinear least squares generally outperformed the linear least squares. The Kalman method outperformed everything else except the result of the nonlinear least squares method on data set 3. To some extent though, the results of the Kalman method were disappointing. Using just the Case 1 data, it should

have equaled the linear least squares, but it did not. Using just 84 data points in the Kalman method improved Case 1 results to an RSS error of 0.0407 but degraded the other results. We do not understand why this is the case, but given more time, it would be interesting to investigate this further. The Kalman method seems to be programmed correctly. We did the runs in reverse sequence, cases 5, 4, 3, 2, and 1 and got the same final results. Also, for a low-noise case, $\sigma_N = 0.005$, the Kalman and linear least-squares methods gave the same results. Perhaps the Kalman and linear least-squares methods are not mathematically equivalent in the presence of noise.

We found a curious result involving the data spacing with these computations. The poles were first extracted using a data spacing of $\Delta t = 0.2857$ nsec giving a Nyquist frequency of 1.75 GHz, which exceeds the highest frequency present, namely 1.71 GHz. All the methods consistently underestimated the magnitudes of the real parts of the last two pole pairs. The Kalman method did not help with this. Apparently the highest frequency was too close to the Nyquist frequency. When Δt was reduced to 0.25 nsec (Nyquist frequency = 2.00 GHz), the results improved greatly, and the errors in the real parts of the last two poles were random.

APPLICATION TO EXPERIMENTAL DATA

Because of problems with the tape recorder we originally planned to use, we had to hand digitize the experimental curves we analyzed and punch the values on cards to feed into the computer. The oscilloscope traces were enlarged to 30.5 x 38.1 cm (12 x 15 in.). The 201 points were hand digitized from each enlargement. Each set of data was interpolated and smoothed to 512 points (at equally spaced time intervals), using a cubic spline routine. This procedure was performed for the returns from the hemisphere, the cylinder, and no object (clutter).

It can be seen from Figure 8 that the returns from the objects had a lot of clutter superimposed on them. This clutter interferes with the analysis of the return to find the poles. If the clutter were just additive, it could be removed by subtracting the object-free return. This was tried but was not very successful. Any reflections arising in the transmitting circuitry are convolved with the impulse response and, thus, cannot be subtracted out. This apparently was the problem here. It might be possible to deconvolve the clutter, if enough information were obtained about its characteristics to allow distinguishing it in some way from the signal.

Tables 3 and 4 show the results of applying the various methods to the cylinder and hemisphere data. The total data span for each was 10 nsec, divided into 511 time steps. This gives a data spacing of 0.01957 nsec. The theory only applies to the free-ringing response of the object, so the first point to be used must be received later than the reflection (if any) of the trailing edge of the pulse from the farthest edge of the object. Since the objects are each 12.7 cm (5 in.) in diameter and the pulse width is about 1 nsec, the time from the beginning of the reflection to the first point to be used is about

$$1 + \frac{2 \times 12.7\text{cm}}{30\text{cm/nsec}} = 1.85 \text{ nsec}$$

Table 3. Poles from Cylinder

Linear-Least Squares		Nonlinear-Least Squares	
Clutter Not Removed (GHz)	Clutter Removed (GHz)	Clutter Not Removed (GHz)	Clutter Removed (GHz)
-0.16 ± j 0.037	-0.14 ± j 0.037	-0.29 ± j 0.038	-0.32 ± j 0.038
-0.75 ± j 0.22	-0.24 ± j 0.11	-0.54 ± j 0.19	-1.88 ± j 0.14
-2.03 ± j 0.38	-0.82 ± j 0.21	-1.24 ± j 0.40	-0.74 ± j 0.21
-2.97 ± j 0.65	-1.09 ± j 0.31	-3.09 ± j 0.65	-0.69 ± j 0.40
-3.13 ± j 0.82	-0.68 ± j 0.37	-2.33 ± j 0.80	-1.73 ± j 1.04
-4.01 ± j 1.02	-6.11 ± j 0.82	-2.16 ± j 1.06	
-2.78 ± j 1.40	-1.56 ± j 1.56	-3.45 ± j 1.26	
		-2.36 ± j 1.41	

Table 3 shows the results of applying the linear and nonlinear least-squares methods to the cylinder data both in its original form and with the clutter subtracted. Table 4 shows the results from applying all three methods to the return from the hemisphere with the clutter subtracted. The least-squares methods used time steps of 0.03914 nsec and 95 data points. The Kalman method used time steps of 0.01957 nsec and 200 data points.

Table 4. Poles from Hemisphere, Clutter Subtracted

Linear-Least Squares	Nonlinear Least Squares	Kalman
$-9.59 \pm j\ 0.11\times10^{-18}$	$-0.29 \pm j\ 0.$	$-0.60 \pm j\ 0.$
$-1.54 \pm j\ 0.17\times10^{-14}$	$-8.33 \pm j\ 0.11\times10^{-14}$	-4.86 ± j 1.23
-1.41 ± j 1.12	-0.80 ± j 1.49	-4.93 ± j 3.32
-1.72 ± j 2.26	-1.83 ± j 2.19	-1.28 ± j 5.78
-2.07 ± j 3.57	-0.07 ± j 3.05	-2.12 ± j 8.08
-1.81 ± j 4.85	-0.003 ± j 5.03	
-0.92 ± j 6.46	-0.37 ± j 6.37	
-2.55 ± j 8.04	-0.08 ± j 7.66	
-3.94 ± j 9.37	-1.25 ± j 8.56	

It can be seen that the results are not very consistent. Since the methods worked well on synthetic data with added random noise, the problem here is apparently due to excessive clutter that is not random and is correlated with the signal. Besides, the clutter cannot be represented as a sum of damped exponentials, which Prony's algorithm demands. If one examines the clutter carefully (Figure 8) and compares it with the impulse generator pulse (Figure 5), one sees that the clutter appears to be a series of reflections or miniature replicas of the impulse generator pulse. We tried Prony's algorithm and the various methods on the impulse generator pulse as received by the TEM horn to check the tolerance of Prony's algorithm to nonexponential waveforms. The results on the impulse generator pulse were totally meaningless. Since the clutter appears to consist of miniature replicas of the impulse generator pulse, we would expect that Prony's algorithm will not work well on such a waveform.

To obtain meaningful results with the presently available techniques, the clutter must be reduced. This can probably be achieved by using fewer and better connectors. Another possible way to deal with the clutter may be to deconvolve it by homomorphic deconvolution techniques.[11] This may work, but only if the frequencies contained in the clutter are vastly different from the frequencies in the returns.

We had intended to do runs similar to those described above on the return from the cone, but in view of the clutter problems, we decided to forgo the cone runs until after the clutter problems are solved.

CONCLUSIONS

The time-domain range and the method for gathering experimental data were described. Prony's algorithm was discussed as a means for processing scattered returns from objects. Improvements in the algorithm were described that help it to better process noisy synthetic data. It did not, however, do well on experimental returns. The main reason was clutter that cannot be represented as a sum of damped sinusoidal waveforms, which Prony's algorithm demands.

The needs for further effort are as follows:

1. Improve experimental techniques so that the data obtained are in a form that can be handled by presently available signal processing techniques. This would include getting rid of clutter and noise as much as possible. Clutter can be reduced by eliminating unnecessary connectors and replacing those needed with connectors that are good at high frequencies (15 GHz and up) to reduce reflections. Also, grounds need to be checked to eliminate ground loops. To reduce noise, we recommend a minicomputer that can control the sweep of the sampling scope. In this way, many samples of the same point can be received and averaged.

2. Improve signal processing techniques so that good results can be obtained from bad (noisy, cluttered) data. This would include intensive parameter studies on Prony's algorithm and seeking ways to deconvolve clutter and noise from the sought for returns. Also, new techniques should be sought and tried.

REFERENCES

1. C. E. Baum, *On the Singularity Expansion Method for the Solution of Electromagnetic Interaction Problems*, Interaction Notes, Note 88, (11 December 1971).

2. R. Prony, "Essai Experimental et Analytique," *J. Ecole Polytechnique*, (Paris, 1795), 1 (2), pp. 24-76.

3. V. C. Martins, J. L. Van Meter, J. M. Proud, and D. J. Fitzgerald, *Picosecond Pulse Reflector Antenna Investigation*, RADC-TR-73-215 (Griffiss Air Force Base, N.Y., July 1973).

4. A. G. Evans and R. Fischl, "Optimal Least Squares Time-Domain Synthesis of Recursive Digital Filters," *IEEE Transactions on Audio and Electroacoustics*, AV-21, (February, 1973), pp. 61-65.

5. J. N. Brittingham, E. K. Miller, and J. L. Willows, *The Derivation of Simple Poles in a Transfer Function from Real-Frequency Information*, UCRL-52050, Lawrence Livermore Laboratory, (6 April 1976), pp. 2-4.

6. R. H. Pennington, *Introductory Computer Methods and Numerical Analysis*, (New York: Macmillan, 1970).

7. F. B. Hildebrand, *Introduction to Numerical Analysis*, (New York: McGraw-Hill, 1974).

8. C. L. Lawson and R. J. Hanson, *Solving Least Squares Problems* (Englewood Cliffs, N.J.: Prentice Hall, 1974).

9. J. L. Junkins, *Optimal Estimation Theory*, NSWC TN-K-45/74 (Dahlgren, Va., January 1975), pp. 19-27.

10. M. L. Van Blaricum and R. Mittra, *"Problems and Solutions Associated with Prony's Method for Processing Transient Data," IEEE Transactions on Antennas and Propagation*, AP-26, (January, 1978), pp. 174-182.

11. S. M. Riad and N. S. Nahman, "Application of the Homomorphic Deconvolution for the Separation of TDR Signals Occurring in Overlapping Time Windows," *IEEE Transactions on Instrumentation and Measurement*, IM-25, (December, 1976), pp. 388-391.

DISTRIBUTION

Naval Air Systems Command
AIR-310B
ATTN: J. W. Willis (2)
Washington, DC 20361

Commanding Officer
Naval Ordnance Station
Gun Systems Engineering Department
ATTN: Technical Library (Code 50D) (2)
Louisville, KY 40214

R. C. Hansen, Inc.
Box 215
Tarzana, CA 91356

Naval Postgraduate School
ATTN: Michael Morgan
Monterey, CA 93940

The Ohio State University
Electro Science Laboratory
1320 Kinnear Road
ATTN: David Moffatt (4)
Eric Walton
Columbus, OH 43212

Office of Naval Research
800 North Quincy Street
Arlington, VA 22217 (2)

Commander
Rome Air Development Center
ATTN: Paul Van Etten
Griffis Air Force Base, NY 13440

Teledyne Micronetics
7155 Mission Gorge Road
ATTN: Steven Weisbrod
San Diego, CA 92120

Director
Naval Research Laboratory
4555 Overlook Avenue, SW
ATTN: Philip Moser
Arthur K. Jordan
Washington, DC 20375

DISTRIBUTION (Continued)

Office of Naval Research
Western Regional Office
1030 East Green Street
Pasadena, CA 91106 (2)

Electronics Engineering Department
University of California
Lawrence Livermore Laboratory
Box 808
ATTN: E. K. Miller (2)
Livermore, CA 94550

Electromagnetics Division
National Bureau of Standards
ATTN: Andy Ondrejka (4)
Norris S. Nahman
Robert A. Lawton
Boulder, CO 80303

General Dynamics
Electronics Division
Box 81127
ATTN: Gus Tricoles
San Diego, CA 92138

Systems Applications
Sperry Corporate Research Center
100 North Road
ATTN: C. Leonard Bennett
Sudbury, MA 01776

Effects Technology, Inc.
Electromagnetics Section
5383 Hollister Avenue
ATTN: Michael L. VanBlarium
Santa Barbara, CA 93111

Picosecond Pulse Labs
8663 Hollyhock Lane
ATTN: James R. Andrews
Lafayette, CO 80026

Department of Electrical Engineering
Texas Tech University
ATTN: Thomas F. Trost
Lubbock, TX 79409

DISTRIBUTION (Continued)

Department of Physics
Catholic University of America
ATTN: Herbert Uberall (2)
Washington, DC 20064

Department of Electrical Engineering
University of Illinois at Chicago Circle
Box 4348 SEO-1104
ATTN: Woffgang M. Boerner
Chicago, IL 60680

Department of Electrical Engineering
Rochester Institute of Technology
One Lomb Memorial Drive
ATTN: Tapan K. Sarkar (2)
George Whitman Reed
Rochester, NY 38677

Department of Electrical Engineering
Michigan State University
ATTN: Kun-Mu Chen
East Lansing, MI 48824

Department of Electrical Engineering
Virginia Polytechnic Institute
ATTN: Sedki M. Riad
Blacksburg, VA 24060

Electromagnetic Radiation Analysis Branch
U. S. Environmental Protection Agency
Office of Radiation Programs
Box 18416
ATTN: Richard A. Tell
Las Vegas, NV 89114

Electromagnetic Sciences Laboratory
SRI International
ATTN: David M. Bubenik
Menlo Park, CA 94025

DISTRIBUTION (Continued)

Defense Technical Information Center
Cameron Station
Alexandria, VA 22314 (12)

Library of Congress
ATTN: Gift and Exchange Division (4)
Washington, DC 20540

Local:

E31 (GIDEP)
E41 (Hall)
F
F10
F12
F12 (Hollmann) (10)
R
X210 (6)


DAT
FILM